RSC Advances

ROYAL SOCIETY OF CHEMISTRY

www.rsc.org/advances

Enhancing low pressure CO_2 adsorption of solvent-free derived mesoporous carbon by highly dispersed potassium species

Baodeng Wang[a,b], Zhongzheng Zhang[a], Chenming Zhu[a], Lina Zhang[a], Nannan Sun[a*], Wei Wei[a*], Yuhan Sun[a,c]

[a] CAS Key Lab of Low-Carbon Conversion Science and Engineering, Shanghai Advanced Research Institute, Chinese Academy of Sciences, Shanghai 201203, China

[b] School of Chemistry and Chemical Engineering, University of Chinese Academy of Sciences, Beijing 100049, China

[c] School of Physical Science and Technology, ShanghaiTech University, Shanghai 201203, China

Abstract

Highly dispersed potassium species were introduced on mesoporous carbon surface following an oxidation and subsequent ion exchange protocol. The samples were characterized and their CO_2 adsorption performance was systematically evaluated by both static and dynamic adsorption tests. It was found that the generated surface functionality can be tuned by controlling the reaction temperature and/or using different oxidant(s), and thus potassium species can be introduced in an adjustable way without significant alteration on the textural properties of the samples. Although adsorption at atmospheric pressure was not influenced, low pressure CO_2 uptake and adsorption selectivity were considerably enhanced by potassium introduction owing to the highly dispersed potassium species. A high CO_2 adsorption capacity of 5.9 wt.% was achieved at 25 ^oC and 0.15 bar with excellent cyclic stability, and the adsorbents can be readily regenerated at 115 ^oC under N_2 purging.

Kew Words: Materials, Carbon, Capture, Adsorption

1. Introduction

The CO_2 concentration in atmosphere has now exceeded 400 ppm, which was believed to be a major contributor to the greenhouse effect and climate change. [1] One approach to tackle the issue is CO_2 capture and storage (CCS), which has been recognized as of vital importance for CO_2 reduction. [2, 3] Currently, CCS is prohibitively expensive, and CO_2 capture represents a major contributor to the total cost.[4, 5] Consequently, development of more efficient process for CO_2 capture is highly desired, especially post-combustion capture (PCC) technology that is more suitable to retrofit with coal- and nature gas-based power plants. In this context, it was proposed that CO_2 adsorption using solid materials might be effective in reducing the huge energy demand required by the regeneration of aqueous amine solution, and thus lowering the total cost of CO_2 capture.[6]

As documented in several recent reviews, a wide range of materials have been prepared and

* Corresponding Author. Tel: 0086-15800688730
E-mail: sunnn@sari.ac.cn (Nannan Sun), weiwei@sari.ac.cn (Wei Wei)

evaluated as CO_2 adsorbents such as zeolite, metal oxide, immobilized amines, carbons, metal organic frameworks (MOFs), etc. [7-10] As for PCC, immobilized amines or MOFs with coordinatively unsaturated metal centers are preferred owing to their stronger affinities towards CO_2, which is important to enhance the adsorption selectivity.[11-13] However, these materials suffered from higher regeneration energy and are more prone to be deactivated due either to irreversible adsorption of contaminants in flue gas (e.g. NO_x and SO_x) or their chemical instability (e.g. oxidative degradation of amines, decomposition of metal-ligand bond in MOFs, etc.).

Carbons are characterized by their large surface areas, low toxicity, and high stability. [14, 15] It has been well demonstrated that porous carbon-based materials are applicable in areas such as adsorption, catalysis, supercapacitor, etc.[14, 16-19] Many efforts have been devoted to prepare carbon-based materials as CO_2 adsorbents, and hetero-atomic dopants, such as nitrogen and sulfur, were used to enhance the adsorption capacities, especially the CO_2 uptake at lower pressures. To this end, a wide range of precursors was used for the preparation of hetero-atom modified carbons, such as chitosan, [20] melamine-phenolic resins,[21] urea modified petroleum coke, [22] polyaniline,[23, 24] polythiophene,[25, 26] polyacrylonitrile (PAN), [27, 28] polypyrrole,[29] and even ionic liquids.[30, 31] For example, Nandi and co-workers prepared N-doped carbons from polyacrylonitrile by carbonization and physical activation, an extraordinary CO_2 uptake of 50.6 wt.% (11.51 mmol/g) was obtained at 273 K and ambient pressure.[28] Zhong et al. used a PAN-containing block copolymer as precursor, the obtained N-enriched carbons exhibited CO_2 uptakes higher than 17.6 wt.% (4 mmol/g) at 273 K.[27] Another precursor worth to mention is polypyrrole, from which carbons with higher nitrogen content can be obtained. For instance, Sevilla reported the KOH activation of polypyrrole to prepare carbons with nitrogen content up to 10.1 wt.%, and the resulted samples were capable to adsorb 27.3 wt.% (6.2 mmol/g) CO_2 at 273 K and 1 bar.[29] Recently, Jaroniec and co-workers reported the use of ethylenediamine as both nitrogen source and catalyst for preparation of carbon microspheres, the obtained samples showed excellent CO_2 uptake of 4.1 mmol/g at 25 ^oC and 1 bar.[32] Most of the above strategy used synthetic polymers as precursors for both the hetero-atom and carbon, this incurred considerable increasing on the costs and environmental footprint of the preparation process. Moreover, it was found that both the surface area of the adsorbents and the content of hetero-atoms affected adsorption capacities of the doped carbons. Oftentimes, a higher carbonization temperature favors the increasing of surface area, however, this also leads to excessive decomposition of the hetero-atom bearing functionalities, and thus lowering their residual contents. This is probably the reason that the low pressure CO_2 uptakes, such as those at 0.15 bar (more relevant to PCC), were still unsatisfied and its enhancement remains a major challenge in the area.

Recently, Zhao et al.[33] reported the enhancement of adsorption performance of carbons by introduction of extra-framework cations, in their work, KOH activation of a pre-synthesized N-containing carbon was carried out, and the as-activated samples were washed with distilled water instead of the normally used HCl solution, a portion of potassium species could thus be introduced into the carbon matrix, and a CO_2 uptake of 7.1 wt.% (1.62 mmol/g) was obtained at 25 ^oC and 0.1 bar. According to their characterization and theoretical calculation, it was concluded that potassium mainly existed in the form of O-K, and this configuration showed a high affinity towards CO_2 molecular. Following similar methodology, our previous work prepared potassium intercalated carbon beads, and CO_2 uptake at 25 ^oC and 0.15 bar achieved 6.6 wt.% (1.51 mmol/g). [34] However, we found that the obtained carbons were mainly microporous probably owing to the

activation effect of KOH,[14, 35] therefore although most the prepared samples possessed large surface areas of ca. 1000 m^2/g, effective potassium loading was limited to ca. 1 wt.%, beyond which the adsorption capacity can hardly change, while lower loadings resulted in less effective samples. This is to say that the potassium washing-off needed to be controlled very carefully, and more importantly, the highly developed porous structure in these samples was not fully utilized.

To circumvent the above issues, we present herein a facile and controllable method for potassium introduction on a mesoporous carbon derived from our previous reported solvent-free method.[36] The pristine carbon was firstly oxidized to generate oxygen-containing functionalities on the surface, potassium ions were subsequently introduced by ion exchange. After further conditioning, carbons with highly dispersed potassium species could be introduced. As compared with the method reported previously,[33, 34] potassium loadings in the current samples can be easily adjusted by controlling the amount of surface oxygen-containing functionalities, which is determined by the reaction temperatures and used oxidant(s). The obtained samples were comprehensively characterized and the adsorption performance was evaluated, it was found that the highly dispersed potassium species could effectively enhance low pressure CO_2 adsorption capacity and selectivity, a high CO_2 uptake of 5.9 wt.% was obtained at 25 ^oC and 1 bar, and the optimized sample showed excellent cyclic stability.

2. Experimental

2.1 Chemicals

Resorcinol and p-phthalaldehyde were obtained from Aladdin Industrial Inc., Pluronic F127 was purchased from Aldrich. Potassium hydroxide, nitric acid and sulfuric acid were obtained from Sinopharm Chemical Reagent Co., Ltd. All chemicals were used without any purification.

2.2 Preparation of Pristine Mesoporous Carbon

Mesoporous carbon (MC) was prepared following an solvent-free method.[36] Typically, 3.00 g of F127, 0.88 g of resorcinol, and 1.12 g of p-phthalaldehyde were evenly mixed and sealed in an autoclave. Then the autoclave was heated to 250 ^oC for 8 h, after which the obtained dark brown solids were carbonized in a N_2 atmosphere at 800 ^oC for 6 h to obtain the final mesoporous carbon (MC).

2.3 Surface Oxidation and Potassium Introduction

To introduce surface functionalities, 3 g of the obtained MC was added in a flask and carefully mixed with 120 ml of concentrated HNO_3 or HNO_3-H_2SO_4 mixture with a volume ratio of 3:1 (mixed-acid, hereafter). After stabilized at ambient conditions for 30 min, the reactants were heated to different temperatures (80, 100 and 110 ^oC) for 8 h to achieve different oxidation degree. The mixture was then cooled down to room temperature, and the solids were recovered by filtration, washed with deionized water, and dried at 120 ^oC overnight. Depending on the used oxidant(s), the oxidized samples were denoted as N***x*** or NS***x***, where N and NS represent nitric acid or mixed acid, respectively, and ***x*** is the oxidation temperature.

The obtained N***x*** and NS***x*** were then submitted to ion exchange with 2M KOH aqueous solution for 24 h, the solids were then filtered, washed with deionized water until neural filtrate was obtained, and dried to afford samples N***x***-K and NS***x***-K. After further annealing at 800 ^oC in a N_2

atmosphere for 6 h, final adsorbents were obtained and denoted as N***x***-K800 and NS***x***-K800, respectively.

2.4 Characterizations

Low temperature (-196 ^{o}C) N_2 physisorption was measured on a Micromeritics Tristar Ⅱ 3020 analyzer to obtain textural properties of the samples, samples were degassed at 120 ^{o}C overnight before any test. Surface area of the samples was calculated by the BET equation, and microporosity was evaluated following the *t-plot* method. Potassium contents were measured by inductive couple plasma (ICP, Optima 8000, Germany), X-ray photoelectron spectroscopy (XPS) was performed on a PHI-5000C ESCA System. The functional groups on the carbon materials surface were also analyzed by fourier transform infrared spectroscopy (FT-IR) and thermal gravimetric analysis (TGA) on ThermoFisher scientific NICOLET 6700 and NETZSH STA 449 F3 analyzer, respectively. Morphology of the samples was investigated using scanning electron microscope (SEM) on a ZEISS EVO18 apparatus, and transmission electron microscope (TEM) was performed on a JEOL 2100F instrument.

2.5 CO_2 Adsorption

CO_2 isotherms were measured on a Micromeritics Tristar Ⅱ 3020 analyzer, and prior to each adsorption measurement, samples were degassed at 120 ^{o}C overnight to remove any physisorbed moistures or other contaminants. Adsorption stability was evaluated by a TGA (TA Q50) with the adsorption and desorption temperatures set at 40 and 115 ^{o}C, respectively, 15 vol.% CO_2 balanced by N_2 with a total pressure of 1bar was used.

3. Results and Discussion

3.1 Surface Functionalization of MC by Liquid Oxidation

Fig. 1a shows the FT-IR spectra of N100 and NS100, from which two well-defined bands at 1710 and 1585 cm^{-1} can be observed. According to literatures,[37, 38] the peak centered at 1710 cm^{-1} is attributable to carboxyl groups involved in aromatic rings, and that at 1585 cm^{-1} may be related to stretching of aromatic rings coupled with highly conjugated C=O moieties. Besides, a broad band at ca. 1200 cm^{-1} can be seen as well, which is assigned to the O–H bending modes. These results indicated clearly that oxygen-containing functionalities could be introduced by the liquid phase oxidation.[39-41] Further, it seems that the mix-acid is a more effective oxidant as the peak intensities are slightly higher than those on the HNO_3 oxidized samples.

Effect of oxidation temperature was further investigated, FT-IR spectra of the samples oxidized in mixed-acid at different temperatures is presented in Fig. 1b. As can be seen, the peak intensity increased with the increasing of oxidation temperature, suggesting higher oxidation level of the carbon surface, and thus higher amounts of surface functionalities can be generated, this could be indicated by TGA as well (Fig. S1), similar trends can also be obtained for the HNO_3 oxidized samples (Fig. S1 and S2). As further evidence, XPS was carried out, and the obtained C1s spectra was showed in Fig. 2, (see Fig. S3 for the N***x*** sample). Peaks attributable to C-C (ca. 284.8±0.1ev), C-O-C (ca. 286.4±0.2 ev), C=O (ca. 287.4±0.2 ev), and O=C-O species (ca. 289.1±0.3 ev) can be observed,[40, 42] indicating again the formation of carboxyl and ether functionalities. In line with the FT-IR results, the peak intensity of O=C-O species increased gradually with the rising of oxidation

temperature suggests the enhancement of surface oxidation.

3.2 Potassium Introduction by Ion-exchange

In order to introduce potassium species onto the carbon surface, the oxidized carbon was treated with KOH solution, it was expected that the induced carboxyl groups could serve as the most preferential site to accommodate K^+ via ion exchange. The above assumption can be evidenced by FT-IR spectra as shown in Fig. 1b (see Fig. S2 for the HNO_3 oxidized series). As can be seen, the intensity of the peaks at 1200 and 1710 cm^{-1} of the NS***x***-K samples decreased generally as compared with the oxidized counterparts probably due to the ion exchange between K^+ and H^+. At the same time, the intensity of the peaks at 1585 cm^{-1} increased, as mentioned above, this band can be related to the stretching of aromatic ring coupled to highly conjugated C=O moieties, since the introduced K^+ is more positively charged as compared with the parent H^+, ion exchange might thus affect the conjugation between the aromatic ring and the carboxyl group, leading to the intensified IR peaks.

Fig. 3 shows the XPS survey of samples after potassium exchange, it can be seen that potassium was successfully induced as K^+ (Fig. S4). Table 1 lists the potassium contents measured by both XPS and ICP, higher values were obtained by XPS for all the samples indicating surface enrichment of potassium, which is reasonable as both oxidation and potassium exchange are supposed to occur on the surface. Moreover, the bulk potassium contents increased with the increasing of oxidation temperature, this can be directly related to the amounts of surface functionalities induced at different temperatures (Fig. S5), which revealed again the preferential attachment of K^+ on the surface functionalities. By using the K^+ ion exchange strategy instead of impregnation, it was expected that the introduced potassium adopted a highly dispersive state, so that the porous structure of the carbon skeleton was not alter significantly, meanwhile, the surface polarity can be enhanced owing to the involving of hetero-atoms, which normally led to improved CO_2 adsorption performance similar to doping carbons with nitrogen or sulfur atoms.[25, 29, 43, 44]

3.3 Textural and Morphological Properties

Fig. 4 and S6 show the low temperature N_2 adsorption isotherms of the samples, as has been reported previously,[36] the parent MC sample exhibited a typical type IV isotherm indicating its mesoporous nature. After oxidation and potassium introduction, similar isotherms can be observed except for the sample NS110 and NS110-K, which showed flat isotherms with considerably lower N_2 uptakes. Pore size distribution (PSD) of the samples was calculated by NLDFT method and showed in Fig. 5 and S7. The parent MC exhibited mesopores with diameters of 2-6 nm, for the oxidized and potassium introduced samples (except NS110 and NS110-K), the porosity at this range slightly decreased while some newly formed larger pores can be found. Akin to the isotherms showed in Fig. 4 and S6, NS110 and NS110-K showed considerably lower pore volumes. It should be mentioned in this work, we focus on the modification of carbon with potassium to enhance low pressure CO_2 adsorption, and it was evidenced that probably most of narrow-micropores (<0.7 nm) were blocked after potassium introduction (see below), therefore narrow-microporosity was not measured.

From Table 2, it can be seen that the parent MC possessed a BET surface area (S_{BET}) of 532 m^2/g and a total pore volume (V_{total}) of 0.32 cm^3/g. Oxidation and potassium introduction generally induced decreasing of textural properties, especially at harsher oxidation conditions. Based on the

above discussion, higher amounts of surface functionalities and potassium species could be introduced upon the use of mixed acid and higher oxidation temperature, it is thus reasonable to conclude that the decreasing of textural properties can be attributed to the damage of basal planes in the carbon matrix, pore blockage by the introduced functionalities/potassium species, or the combination of the two factors. Nevertheless, the detrimental effect of guest loading in porous materials can be properly avoided as most of the samples possessed surface areas higher than 350 m^2/g, which is closely related to the highly dispersed potassium species derived from ion exchange rather than impregnation, as can be demonstrated by the considerable lower N_2 uptake and BET surface area of impregnation-derived samples with similar or even lower potassium loading (Fig. S8, note the potassium content increased significantly after thermal treatment as it is discussed in the following section).

Fig. 6 presents the TEM images of MC and the NS100 series at each preparation step. Porous structure with worm-like morphology can be observed for all the samples, suggesting the carbon matrix stayed intact during the surface treatment which is in line with the N_2 physisorption results. Furthermore, although a significant amount of potassium can be detected on NS100-K (insert of Fig. 6c), very uniform image contrast was obtained for the potassium-containing samples (NS100-K and NS100-K800). This strongly evidenced the highly dispersive state of K^+ on the sample, even after thermal treatment at 800 ^oC.

3.4 CO_2 Adsorption

It has been well demonstrated that gas adsorption on carbon-based materials can be significantly affected by porosity. Especially, narrower pores are favored owing to overlap of surface potential from both the pore walls, and the effective pore size is pressure dependent, for example, it was reported that at atmospheric pressure, only pores with diameters smaller than 5 times of the adsorbate molecular size are effective for gas adsorption.[45] CO_2 has a dynamic molecular diameter of 0.209 nm, this is to say that only narrow micropores are the major locations that accommodate CO_2 at 1 bar.[46] On the other hand, involving of surface functionality can enhance the interaction between CO_2 molecular with the surface, leading to improved adsorption capacity especially at lower pressures.[11, 12, 29, 33, 47]

Fig. 7 shows the CO_2 adsorption isotherms (25 ^oC) of the current samples. It seems that the surface modification induced limited variation on the adsorption capacities at 1 bar, all the materials provided fairly poor performance of no more than ca. 10 wt.%, these values are nearly 50% lower than the best reported carbon materials to date,[22, 25, 48] according to the previous discussion, this is probably owing to the relatively low surface areas and micropore volumes as compared with those microporous carbons reported in the literatures. At a pressure of 0.15 bar however (more relevant to PCC from pulverized coal power plant), the adsorption capacity can be improved considerably after potassium introduction (Table 2). Moreover, as shown in Fig. S9, higher amounts of incorporated potassium can generally lead to higher CO_2 uptakes. Note that a significant increase in the potassium content in the samples after thermal treatment was observed if one compares the data in Fig. S9 and Table 1, which can be explained by the removal of carboxyl groups, partial gasification of the carbon matrix by the activation effect of potassium, or a combination of both effects. Although the surface potassium contents in NS100-K800 and NS110-K800 are close, their CO_2 uptakes differ considerably. Based on this observation, it may be difficult to identify an "optimum" potassium loading, however, the current results indicate that

the high dispersion of potassium species achieved by ion-exchange is well-preserved in the thermally treated samples under the conditions used in this study. Among the prepared samples, NS100-K800 showed a CO_2 uptake of 5.9 wt.% (25 ^oC, 0.15 bar), which is among the highest values reported so far (Table S1) at similar conditions, note that the precursor of the current carbon (phenolic resin) is relatively cheap and easy to prepare in comparison with other synthetic polymers, we thus believe the sample represents a promising low pressure CO_2 adsorbent.

Worth to mention here is the sample NS110-K800 which possessed the highest potassium content, its low performance can be related reasonably to its low surface area, and thus low dispersion of potassium species. In fact, additional detrimental effect of the poor dispersion of potassium can be evidenced by considering the even lower surface area as observed in the sample NS110, which however, showed greater CO_2 uptakes than that of NS110-K800. This indicates the severe blocking of narrow micropores (more efficient in low pressure CO_2 adsorption.[49]) by potassium as compared with surface functionalities in NS100. Similar reason may also be responsible to the small difference in CO_2 uptake at 1 bar among the prepared samples, namely with the increasing of potassium content, the enhanced surface affinity towards CO_2 was balanced by the gradually blocked narrow micropores, leading to small variation on 1 bar CO_2 adsorption.

Based on the above, both a high potassium loading and its high dispersion are of vital importance, and thus the controllable preparation protocol of oxidation followed by K^+ exchange played a decisive role in enhancing the low pressure adsorption performance.

In our previous work, a CO_2 uptake of 6.6 wt.% (25 ^oC, 0.15 bar) was achieved on an optimized sample with only ca. 1 wt.% potassium loading, further increasing of potassium contents led to little increase of the capacity probably due to the microporous nature of the samples. In the current study, although the CO_2 uptake is lower, the effective potassium loading increased significantly without any compromise on its high dispersive feature, this paved a way to further optimization since increasing of effective potassium loading represents an important strategy to achieve higher CO_2 uptakes at low pressures, and we are working on manipulating pore diameter of the pristine carbons to identify more effective adsorbents.

Fig. 8 compares the CO_2 and N_2 adsorption isotherms (25 ^oC) on the pristine MC and NS100-K800, it can be seen that the CO_2 uptakes are considerably higher than N_2 owing to higher quadruple moment and polarizability of CO_2 (13.4×10^{-40} C m^2 and 26.3×10^{-25} cm^3, respectively) as compared to N_2 (4.7×10^{-40} C m^2 and 17.7×10^{-25} cm^3, respectively).[50] Moreover, for the adsorption of N_2, porous properties of an adsorbent represented a more important factor rather than the surface chemistry owing to the inertness of N_2, as a result, sample NS100-K800 exhibited lower N_2 uptake as compared with MC. Here, the adsorption capacity ratio of CO_2 to N_2 was calculated and used as an indicator for the selectivity of the samples, and values of 6.72 and 12.33 were obtained for MC and NS100-K800 at 1 bar, respectively. This suggests that the introduction of potassium can also benefit the surface affinity towards CO_2, resulting in a higher adsorption selectivity. Similar calculation was conducted by using the gas uptakes at 0.15 bar as well, even higher enhancement can be obtained as NS100-K800 showed a 3-fold higher selectivity as compared with MC (37.59 *vs* 12.00).

The cyclic stability of NS100-K800 was further investigated by using a TGA apparatus. In order to simulate the practical CO_2 capture from coal-based power plant, a feeding of 15 vol.% CO_2 balanced with N_2 was used, and the adsorption and desorption temperature were set to be 40 and 115 ^oC, respectively. Fig. 9a presents the weight gain and loss curve during cyclic adsorption and

desorption, a steep increasing of sample weight was observed upon the exposure to CO_2/N_2, and adsorption capacity reached 90% of the final value within about 4 min, indicating fast adsorption kinetics. Similarly, desorption can be easily achieved by N_2 purge at 115 ^oC. The adsorption capacity during the cyclic testing is showed in Fig. 9b, after slight decay during the first 10 cycles, CO_2 capacity of the sample maintained at ca. 4.3 wt.% in the following 40 cycles, this demonstrated the excellent stability of the samples.

Recently, K_2CO_3-based adsorbents were widely reported for CO_2 capture by the reversible reaction of K_2CO_3 carbonation to $KHCO_3$ and the decomposition of the latter (Eq. 1).[51, 52]

$$K_2CO_3 + H_2O + CO_2 = 2KHCO_3 \quad (1)$$

Given the involving of potassium in the current samples, one may assume that Eq. 1 represents the major adsorption mechanism. However, this may not be the case because in this study, all the adsorption experiments were carried out in dry conditions, while presence of water is necessary for the formation of intermediate phases (e.g. $K_2CO_3 \cdot 1.5H_2O$) in K_2CO_3 carbonation.[52, 53] Moreover, the regeneration temperature used in Fig. 9a cannot effectively decompose $KHCO_3$,[54] which means adsorption stability of K_2CO_3 in the current condition should be low. Based on the above, we come to the conclusion that the improving of low pressure CO_2 adsorption in the current carbons originates from the enhancement of surface polarity by the highly dispersed potassium species (mainly intercalated K^+ or O^--K^+ moieties), and thus the modified surface possessed a stronger affinity towards CO_2 leading to the promising adsorption capacity at low pressures. Meanwhile, the adsorption process is physisorption in nature, therefore the adsorbents can be regenerated easily at 115 ^oC and re-used in multi-cycles.

Conclusions

Carbon-based material with excellent low pressure CO_2 adsorption capacity was prepared by surface oxidation and subsequent potassium introduction. According to the combined results from FT-IR, XPS, and TGA, treating the pristine mesoporous carbon by liquid oxidation generated surface functionalities (mainly carboxyl groups) which played an important role in accommodating potassium ions during the ion exchange. This led to the formation of highly dispersed potassium species with minimized detriment on porosity of resulted samples, and loading of potassium could be adjusted by controlling the oxidation agent(s) and conditions. The introduction of highly dispersed potassium had a promoting effect on both the low pressure adsorption capacity (although CO_2 uptakes at 1 bar were not altered significantly owing to the balance between porosity and potassium involving) as well as selectivity towards CO_2 due to the enhancement of surface polarity by the formed O-K configuration. The optimized sample, NS100-K800, showed a CO_2 uptake of 5.9 wt.% at 25 ^oC and 0.15 bar, which is among the highest values reported so far at similar conditions. Meanwhile, good cyclic stability was observed in simulated flue gas capture application, and the adsorbents could be easily regenerated by purging with N_2 at 115 ^oC. The above results indicated that the current approach represents a facile, yet effective methodology in enhancing low pressure CO_2 adsorption of carbon materials.

Acknowledgements

N. Sun wishes to acknowledge the financial support from the "Youth Innovation Promotion Association, CAS".

Reference

1. C. Lastoskie, *Science*, 2010, 330, 595-596.
2. R. K. Pachauri, A. Reisinger and eds, *Geneva, Switzerland: United Nations Intergovernmental Panel on Climate Change*, 2014.
3. International Energy Agency. Technology roadmap: carbon capture and storage. http://www.iea.org/publications/freepublications/publication/TechnologyRoadmapCarbonCaptureandStorage.pdf. Published 2013. Accessed Aug 6, 2015.
4. M. E. Boot-Handford, J. C. Abanades, E. J. Anthony, M. J. Blunt, S. Brandani, N. Mac Dowell, J. R. Fernandez, M. C. Ferrari, R. Gross, J. P. Hallett, R. S. Haszeldine, P. Heptonstall, A. Lyngfelt, Z. Makuch, E. Mangano, R. T. J. Porter, M. Pourkashanian, G. T. Rochelle, N. Shah, J. G. Yao and P. S. Fennell, *Energy Environ. Sci.*, 2014, 7, 130-189.
5. G. T. Rochelle, *Science*, 2009, 325, 1652-1654.
6. D. C. Miller, J. T. Litynski, L. A. Brickett and B. D. Morreale, *AIChE Journal*, 2016, 62, 2-10.
7. S. Choi, J. H. Drese and C. W. Jones, *ChemSusChem*, 2009, 2, 796-854.
8. Q. A. Wang, J. Z. Luo, Z. Y. Zhong and A. Borgna, *Energy Environ. Sci.*, 2011, 4, 42-55.
9. Q. Wang, J. F. Bai, Z. Y. Lu, Y. Pan and X. Z. You, *Chem. Commun.*, 2016, 52, 443-452.
10. F. Shakerian, K. H. Kim, J. E. Szulejko and J. W. Park, *Appl. Energy*, 2015, 148, 10-22.
11. P. Bollini, S. A. Didas and C. W. Jones, *J. Mater. Chem.*, 2011, 21, 15100-15120.
12. A. Sayari, Y. Belmabkhout and R. Serna-Guerrero, *Chemical Engineering Journal*, 2011, 171, 760-774.
13. K. Sumida, D. L. Rogow, J. A. Mason, T. M. McDonald, E. D. Bloch, Z. R. Herm, T. H. Bae and J. R. Long, *Chem. Rev.*, 2012, 112, 724-781.
14. J. C. Wang and S. Kaskel, *J. Mater. Chem.*, 2012, 22, 23710-23725.
15. C. Zhang, W. Lv, Y. Tao and Q. H. Yang, *Energy Environ. Sci.*, 2015, 8, 1390-1403.
16. J. Ryu, N. Jung, D. H. Lim, D. Y. Shin, S. H. Park, H. C. Ham, J. H. Jang, H. J. Kim and S. J. Yoo, *Chem. Commun.*, 2014, 50, 15940-15943.
17. M. S. Balogun, Y. Luo, W. T. Qiu, P. Liu and Y. X. Tong, *Carbon*, 2016, 98, 162-178.
18. T. Q. Lin, I. W. Chen, F. X. Liu, C. Y. Yang, H. Bi, F. F. Xu and F. Q. Huang, *Science*, 2015, 350, 1508-1513.
19. J. Liu, N. P. Wickramaratne, S. Z. Qiao and M. Jaroniec, *Nat. Mater.*, 2015, 14, 763-774.
20. F. Xiangqian, Z. Lingxia, Z. Guobin, S. Zhu and S. Jianlin, *Carbon*, 2013, 61, 423-430.
21. C. Chen, J. Kim and W. S. Ahn, *Fuel*, 2012, 95, 360-364.
22. B. Ruizhu, Y. Mingli, H. Gengshen, X. Leqiong, H. Xin, L. Zhiming, W. Sunli, D. Wei and F. Maohong, *Carbon*, 2015, 81, 465-473.
23. L. M. Zhang, Z. B. Wang, J. J. Zhang, X. L. Sui, L. Zhao and D. M. Gu, *Carbon*, 2015, 93, 1050-1058.
24. A. K. Mishra and S. Ramaprabhu, *RSC Adv.*, 2012, 2, 1746-1750.
25. H. Seema, K. C. Kemp, N. H. Le, S. W. Park, V. Chandra, J. W. Lee and K. S. Kim, *Carbon*, 2014, 66, 320-326.
26. X. Yongde, Z. Yanqiu and T. Yi, *Carbon*, 2012, 50, 5543-5553.
27. M. J. Zhong, S. Natesakhawat, J. P. Baltrus, D. Luebke, H. Nulwala, K. Matyjaszewski and T. Kowalewski, *Chem. Commun.*, 2012, 48, 11516-11518.
28. M. Nandi, K. Okada, A. Dutta, A. Bhaumik, J. Maruyama, D. Derks and H. Uyama, *Chem.*

Commun., 2012, 48, 10283-10285.
29. M. Sevilla, P. Valle-Vigon and A. B. Fuertes, *Adv. Funct. Mater.*, 2011, 21, 2781-2787.
30. G. Sethia and A. Sayari, *Energy Fuels*, 2014, 28, 2727-2731.
31. X. Zhu, P. C. Hillesheim, S. M. Mahurin, C. M. Wang, C. C. Tian, S. Brown, H. M. Luo, G. M. Veith, K. S. Han, E. W. Hagaman, H. L. Liu and S. Dai, *ChemSusChem*, 2012, 5, 1912-1917.
32. N. P. Wickramaratne, J. T. Xu, M. Wang, L. Zhu, L. M. Dai and M. Jaroniec, *Chem. Mat.*, 2014, 26, 2820-2828.
33. Y. F. Zhao, X. Liu, K. X. Yao, L. Zhao and Y. Han, *Chem. Mat.*, 2012, 24, 4725-4734.
34. J. J. Liu, N. N. Sun, C. G. Sun, H. Liu, C. Snape, K. X. Li, W. Wei and Y. H. Sun, *Carbon*, 2015, 94, 243-255.
35. J. Ludwinowicz and M. Jaroniec, *Carbon*, 2015, 94, 673-679.
36. Z. Z. Zhang, B. D. Wang, C. M. Zhu, P. Gao, Z. Y. Tang, N. N. Sun, W. Wei and Y. H. Sun, *Journal of Materials Chemistry A*, 2015, 3, 23990-23999.
37. A. Macías-García, M. A. Díaz-Díez, E. M. Cuerda-Correa, M. Olivares-Marín and J. Gañan-Gómez, *Applied Surface Science*, 2006, 252, 5972-5975.
38. C. Moreno-Castilla, M. V. Lopez-Ramon and F. Carrasco-Marin, *Carbon*, 2000, 38, 1995-2001.
39. A. M. Dimiev, S. M. Bachilo, R. Saito and J. M. Tour, *ACS Nano*, 2012, 6, 7842-7849.
40. H. P. Boehm, *Carbon*, 2002, 40, 145-149.
41. M. G. Plaza, K. J. Thurecht, C. Pevida, F. Rubiera, J. J. Pis, C. E. Snape and T. C. Drage, *Fuel Processing Technology*, 2013, 110, 53-60.
42. J. P. McClure, R. Z. Jiang, D. Chu and P. S. Fedkiw, *Carbon*, 2014, 79, 457-469.
43. J. Song, W. Z. Shen, J. G. Wang and W. B. Fan, *Carbon*, 2014, 69, 255-263.
44. W. G. Lu, D. Q. Yuan, J. L. Sculley, D. Zhao, R. Krishna and H. C. Zhou, *J. Am. Chem. Soc.*, 2011, 133, 18126-18129.
45. M. M. Maroto-Valer, Z. Tang and Y. Z. Zhang, *Fuel Processing Technology*, 2005, 86, 1487-1502.
46. A. Hui, F. Bo and S. Shi, *Carbon*, 2009, 47, 2396-2405.
47. L. Wan, J. Wang, C. Feng, Y. Sun and K. Li, *Nanoscale*, 2015, 7, 6534-6544.
48. A. Alabadi, S. Razzaque, Y. W. Yang, S. Chen and B. Tan, *Chemical Engineering Journal*, 2015, 281, 606-612.
49. N. P. Wickramaratne and M. Jaroniec, *Journal of Materials Chemistry A*, 2013, 1, 112-116.
50. Y. S. Bae and C. H. Lee, *Carbon*, 2005, 43, 95-107.
51. H. C. Luo, H. Chioyama, S. Thurmer, T. Ohba and H. Kanoh, *Energy Fuels*, 2015, 29, 4472-4478.
52. Z. Chuanwen, G. Yafei, L. Changhai and L. Shouxiang, *Chemical Engineering Journal*, 2014, 254, 524-530.
53. C. W. Zhao, X. P. Chen and C. S. Zhao, *Energy Fuels*, 2012, 26, 1401-1405.
54. C. W. Zhao, X. P. Chen and C. S. Zhao, *Energy Fuels*, 2009, 23, 4683-4687.

Captions of the illustration

- **Table 1 Potassium contents of the samples after ion exchange**
- **Table 2 Textural properties and CO_2 adsorption capacities**
- **Fig. 1 FT-IR spectra of oxidized samples. (a) Effect of oxidant(s), (b) Effect of oxidation temperatures**
- **Fig. 2 C1s XPS spectra of the NS*x* samples**
- **Fig. 3 XPS survey of NS*x*-K**
- **Fig. 4 Low temperature N_2 isotherms. (a) MC and N*x*-K800, (b) MC and NS*x*-K800**
- **Fig. 5 NLDFT pore size distribution. (a) MC and N*x*-K800, (b) MC and NS*x*-K800**
- **Fig. 6 TEM images of (a) MC, (b) NS100, (c) NS100-K, and (d) NS100-K800**
- **Fig. 7 CO_2 adsorption isotherms at 25 ^{o}C. (a) MC and N*x*-K800, (b) MC and NS*x*-K800**
- **Fig. 8 Comparison of CO_2 and N_2 adsorption isotherms at 25 ^{o}C. (a) MC, (b) NS100-K800**
- **Fig. 9 CO_2 adsorption/desorption cycles on NS100-K800 (15% CO_2, 40 ^{o}C). (a) Weight gain and loss curve, (b) Adsorption capacity during multi-cycles**

1 Table 1 Potassium contents of the samples after ion exchange

Sample	K^+ contents (wt.%)	
	ICP	XPS
N80-K	4.43	6.6
N100-K	6.25	8.0
N110-K	7.93	8.9
NS80-K	5.20	8.2
NS100-K	7.14	9.6
NS110-K	9.86	13.7

2

Table 2 Textural properties and CO_2 adsorption capacities

Sample	S_{BET} (m^2/g)	S_{mic} (m^2/g)	V_{total} (cm^3/g)	V_{mic} (cm^3/g)	CO_2 uptake (wt.%, 25 °C)	
					0.15 bar	1 bar
MC	532	325	0.32	0.13	3.3	8.8
N80	506	308	0.28	0.13	3.9	9.0
N80-K800	511	299	0.31	0.12	4.5	9.5
N100	516	317	0.28	0.13	3.8	9.5
N100-K800	508	252	0.32	0.09	4.9	10.0
N110	517	311	0.28	0.13	3.7	9.1
N110-K800	338	160	0.28	0.05	5.2	9.3
NS80	433	251	0.25	0.10	3.5	8.9
NS80-K800	395	211	0.29	0.08	5.1	9.4
NS100	498	296	0.29	0.12	3.7	9.1
NS100-K800	360	175	0.29	0.06	5.9	10.5
NS110	55	33	0.02	0.01	3.1	7.1
NS110-K800	89	61	0.04	0.03	1.0	1.8

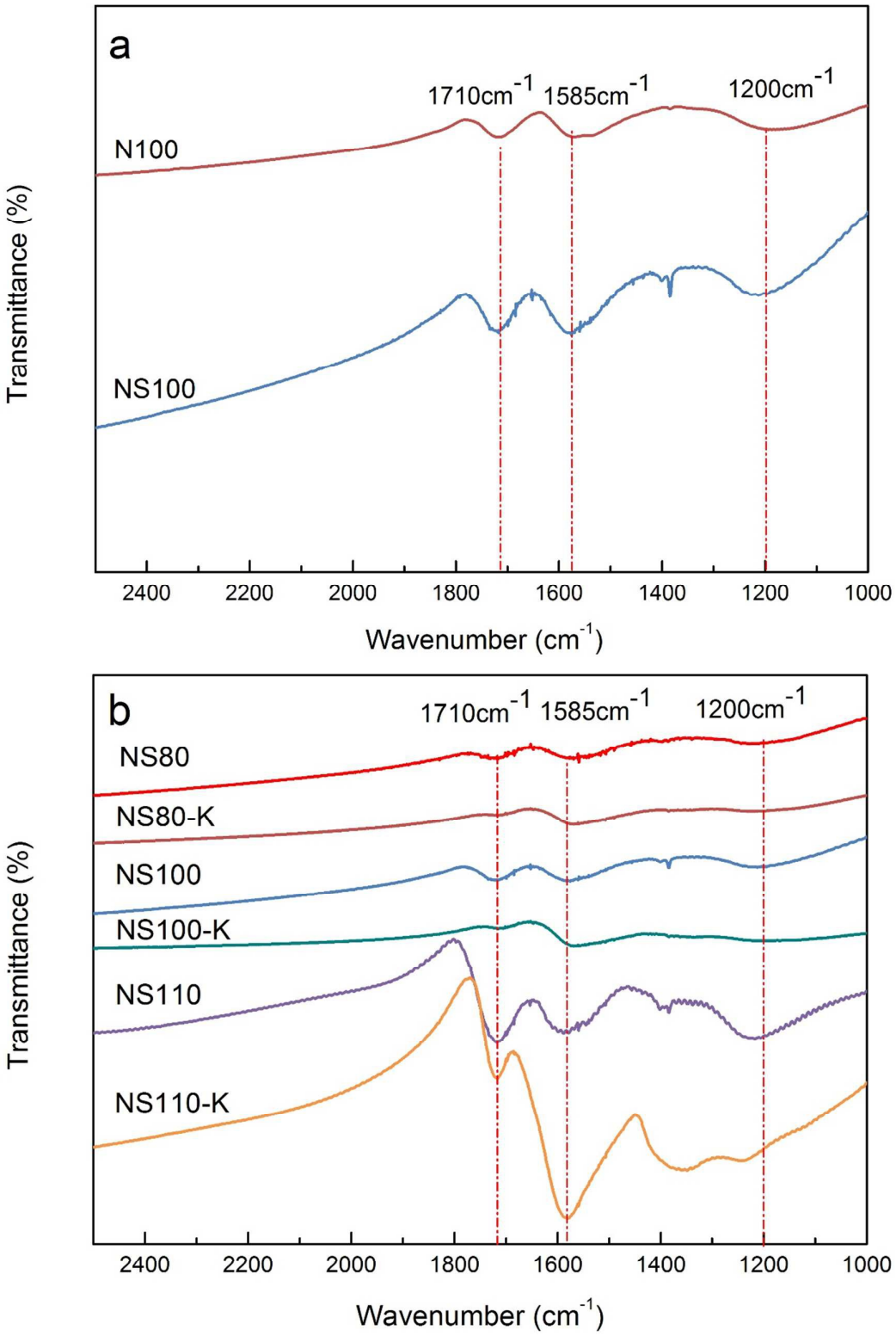

Fig. 1 FT-IR spectra of oxidized samples.
(a) Effect of oxidant(s), (b) Effect of oxidation temperatures

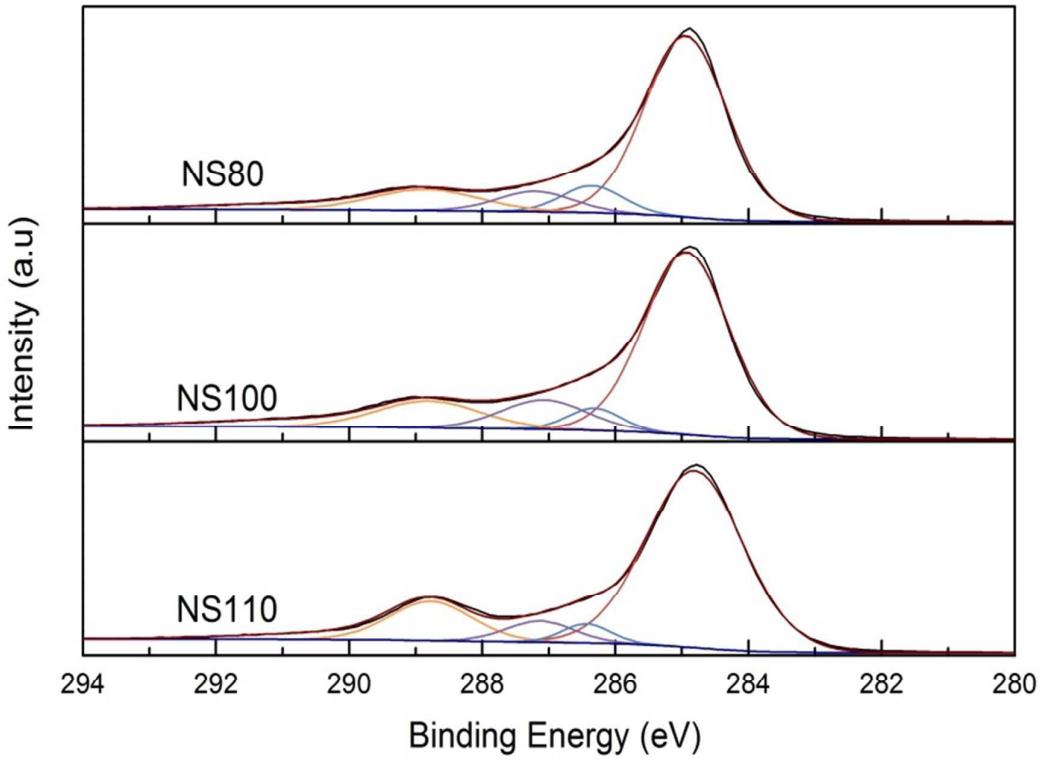

Fig. 2 C1s XPS spectra of the NS*x* samples

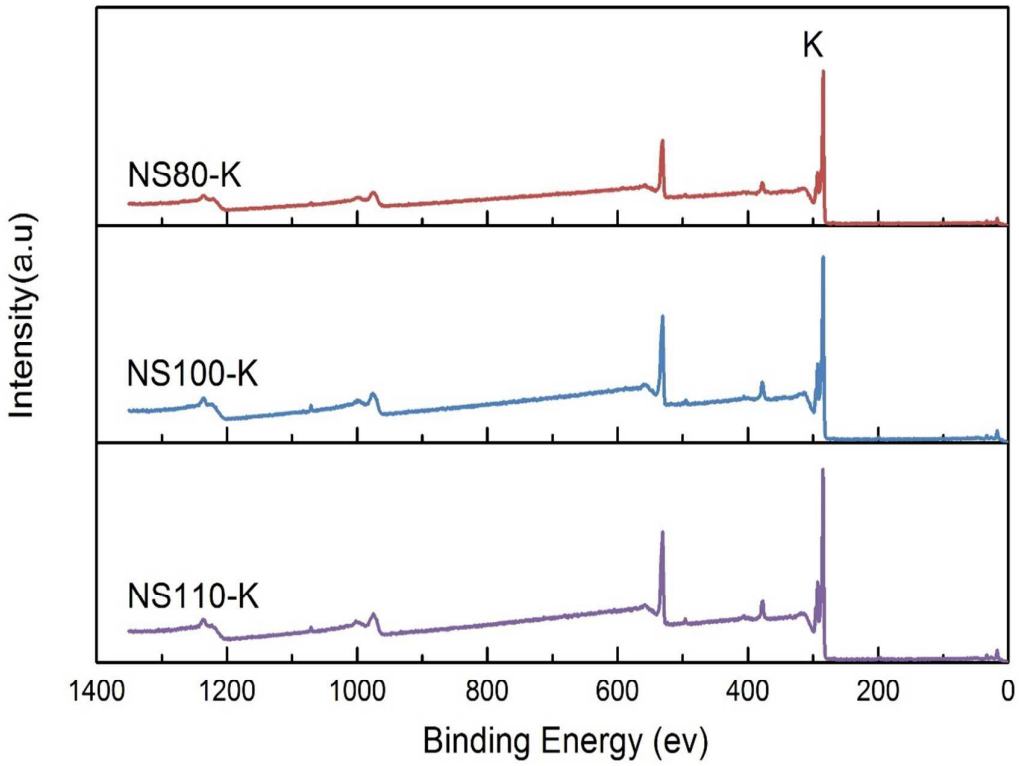

Fig. 3 XPS survey of NS*x*-K

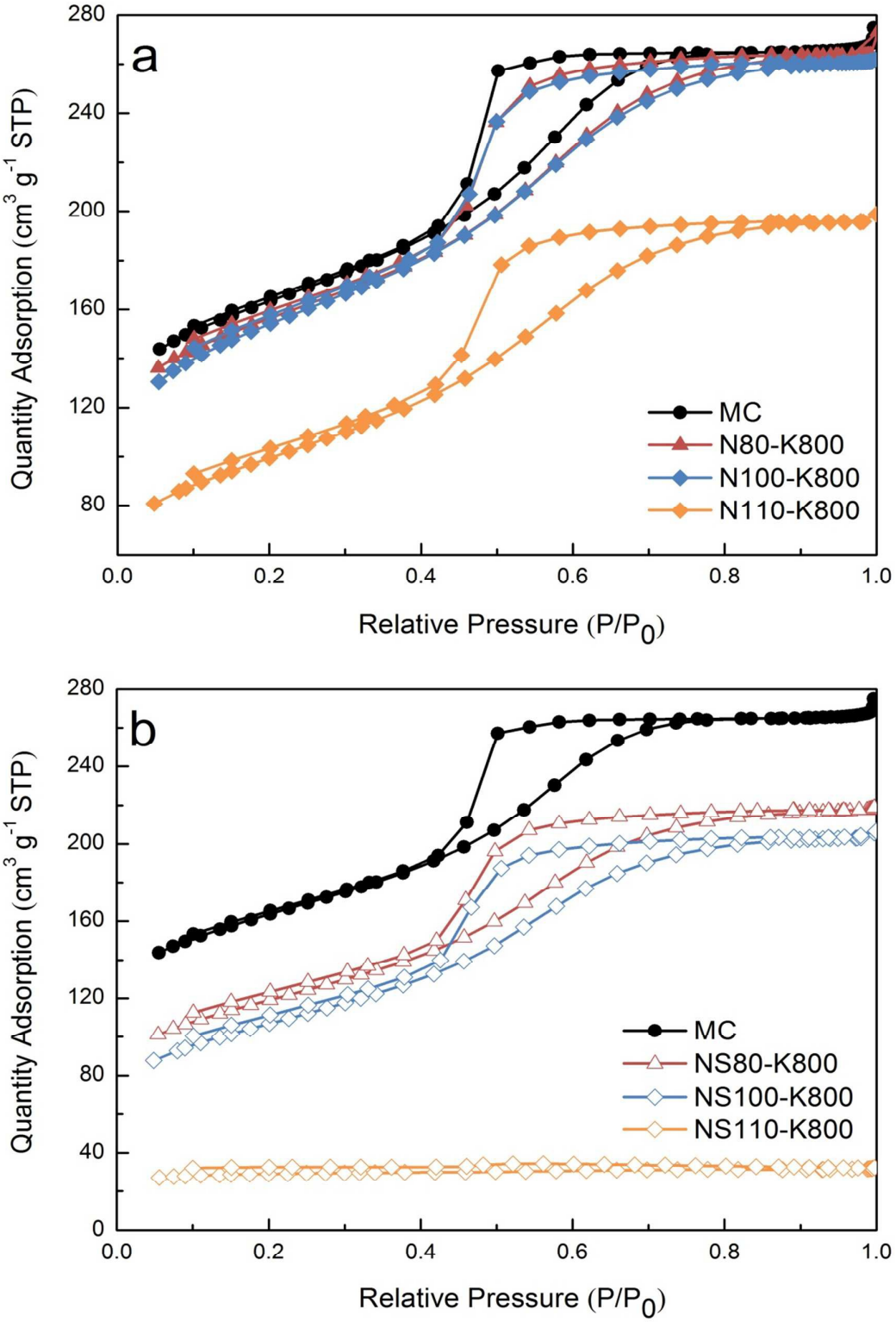

Fig. 4 Low temperature N_2 isotherms. (a) MC and N***x***-K800, (b) MC and NS***x***-K800

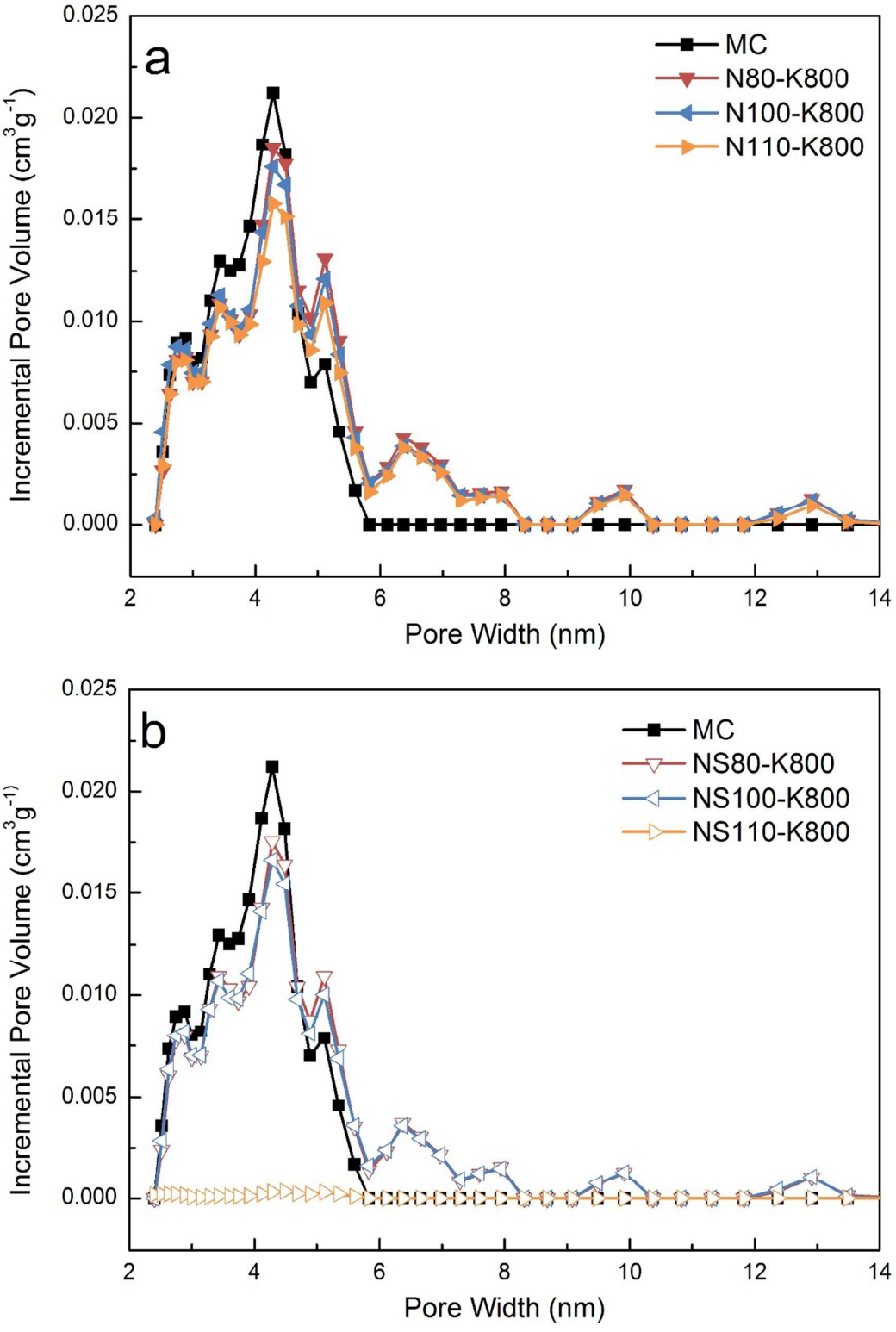

Fig. 5 NLDFT pore size distribution. (a) MC and N*x*-K800, (b) MC and NS*x*-K800

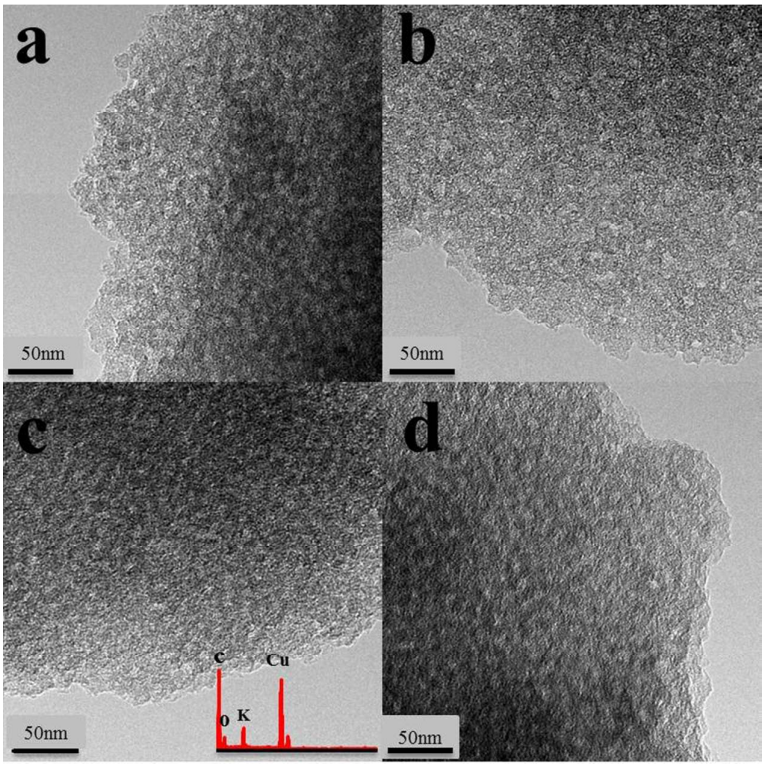

Fig. 6 TEM images of (a) MC, (b) NS100, (c) NS100-K, and (d) NS100-K800

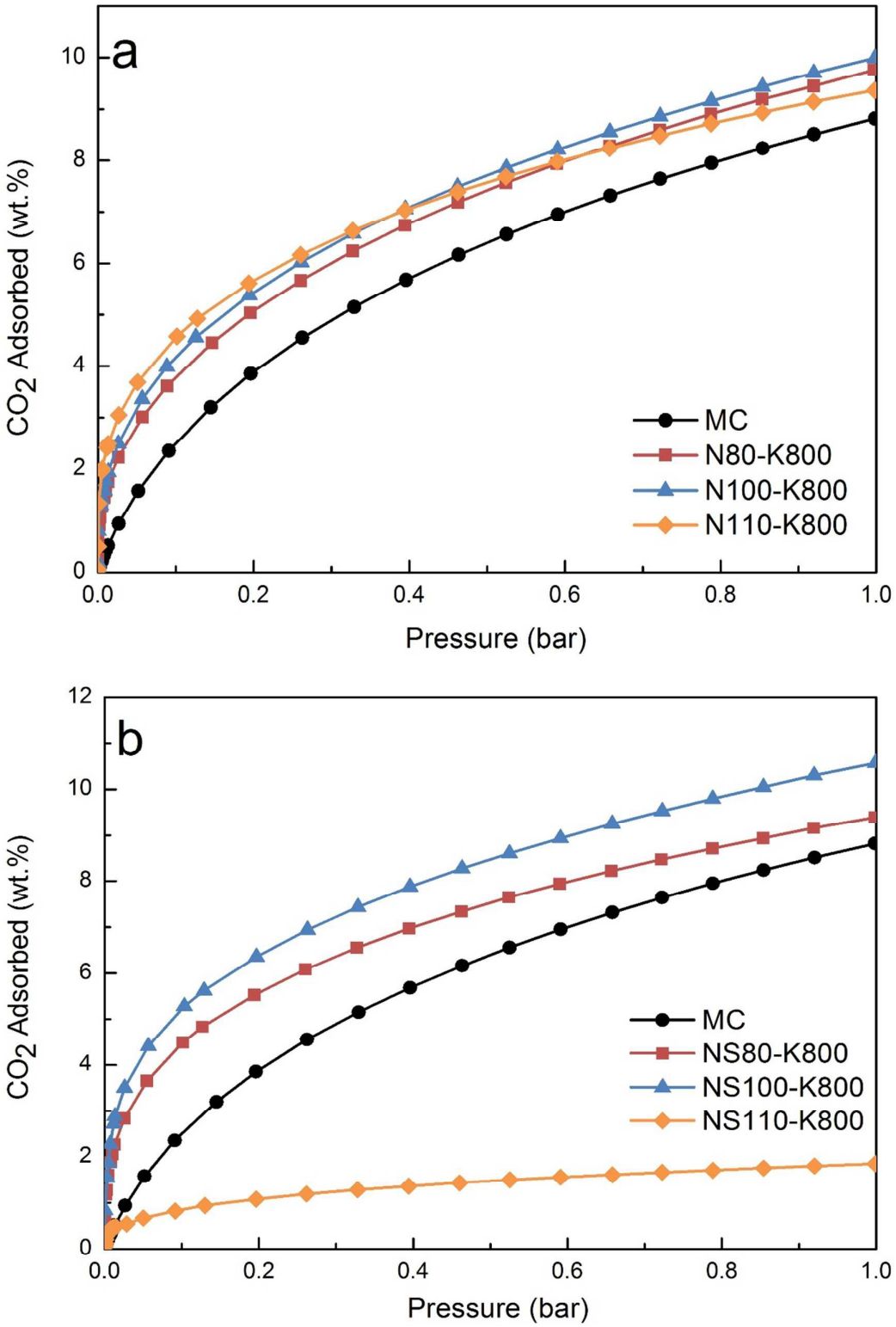

Fig. 7 CO_2 adsorption isotherms at 25 °C.
(a) MC and N*x*-K800, (b) MC and NS*x*-K800

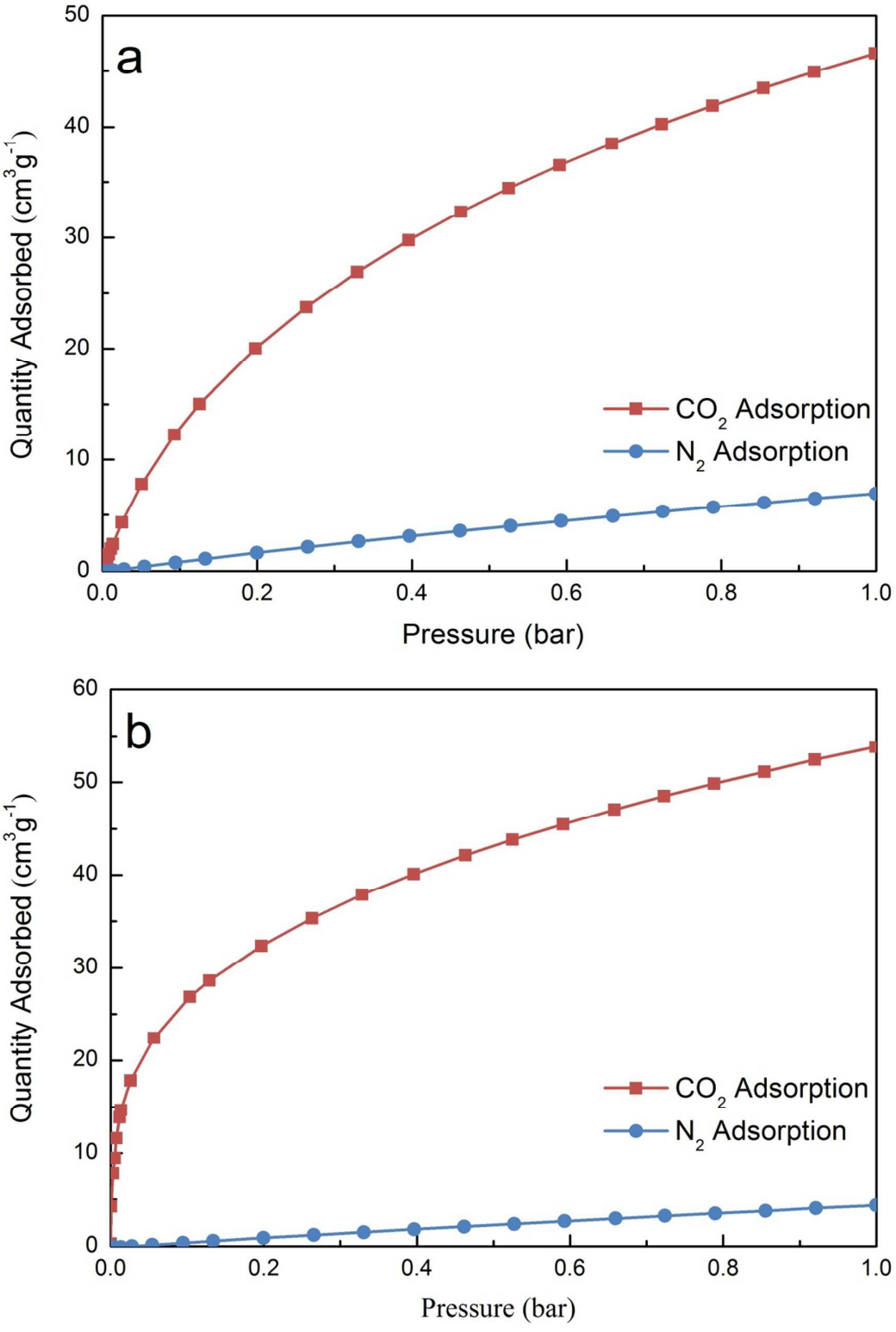

Fig. 8 Comparison of CO_2 and N_2 adsorption isotherms at 25 ^{o}C.
(a) MC, (b) NS100-K800

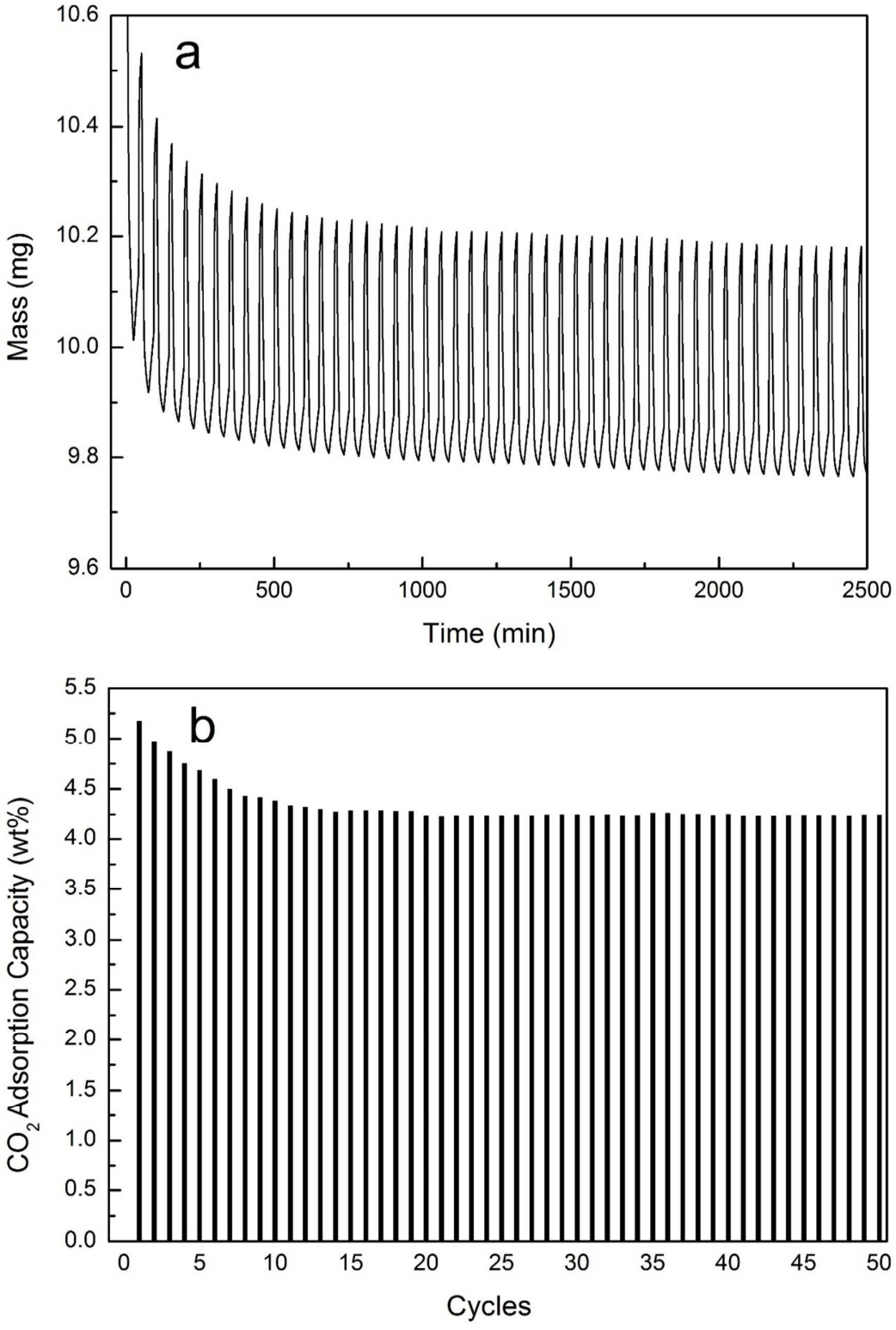

Fig. 9 CO_2 adsorption/desorption cycles on NS100-K800 (15% CO_2, 40 ^oC).
(a) Weight gain and loss curve, (b) Adsorption capacity during multi-cycles